DOI: 10.1002/chem.201001301

Imaging the Oxidation of ZnS Encapsulated in Carbon Nanotubes

Pedro M. F. J. Costa,*[a] Thomas W. Hansen,[b] Jakob B. Wagner,[b] and Rafal E. Dunin-Borkowski[b]

Diffusion is a common process in binary and compound materials at elevated temperature. Due to the different diffusion rate of each component, vacancies can form and coalesce, leading ultimately to the appearance of voids in a heterogeneous solid. The proposal that diffusion in solids occurs by a vacancy migration mechanism[1] has fascinated metallurgists, materials scientists and chemists for decades. Recently, this so-called "Kirkendall effect" has been used to explain the formation of a number of hollow nanoparticles[2,3] and nanotubes.[4,5] However, due to their dimensions, it has been difficult to characterise the "solid-to-hollow" transformations that take place in these nanostructures. Invariably, mechanistic assumptions have been supported by "post-mortem" observations of representative nanostructures after specific reaction times.[6,7] In order to observe a single nanostructure and to follow such changes, in situ characterisation techniques that have nanometre spatial resolution and a temporal resolution on the order of milliseconds are required. The transmission electron microscope (TEM) is a powerful analytical tool that can provide both high-spatial-resolution structural images and video-rate recording of dynamic processes. In addition, the development of reaction chambers and advances in electron optics has enabled the emergence of a new category of instruments, which are termed aberration-corrected environmental TEMs. This capability now provides the opportunity to follow gas–solid reactions with improved spatial and temporal resolution.

In this communication, the dynamics of the Kirkendall effect in a nanocable-to-nanotube transition are followed on a sub-second timescale in a TEM, for individual nanostructures of turbostratic C nanotubes filled with Ga-doped ZnS ($Zn_{0.92}Ga_{0.08}S$@CNT).

The synthesis of the filled nanotubes (i.e., nanocables) used here has been described previously.[8] In the same report, it was revealed how tubular heterostructures of ZnO and $ZnGa_2O_4$ grains could be obtained through the controlled oxidation of $Zn_{0.92}Ga_{0.08}S$@CNT. The nanocable-to-nanotube transition was then carried out using normal bench techniques. Despite the wide distribution of diameters of the starting material (60 to 160 nm), the reaction was ubiquitous and resulted in the formation of oxidised structures with diameters ranging from 140 to 280 nm. On the basis of observations of the products after different reaction times, the Kirkendall effect was proposed as the driving mechanism underlying the transition. However, definitive evidence to support this assumption for individual nanostructures was lacking. Here, we endeavour to reproduce the oxidation process in a reactor with in situ analytical capabilities, in an FEI Titan™ environmental TEM (ETEM).

Experimental conditions in the ETEM were similar to those described in reference [8] wherever possible. A pure oxygen atmosphere was used and the range of specimen temperatures employed differed by a maximum of 10% from those implemented previously ($\approx$550 °C). Pressures and flow rates were modified due to instrumental requirements (see experimental conditions and Figures S1 and S2 in the Supporting Information). Despite a period of almost two years since the original synthesis, as well as the absence of measures to protect the materials from contaminants, the starting $Zn_{0.92}Ga_{0.08}S$@CNTs were found to be structurally and compositionally preserved (Figure S3 in the Supporting Information).

Control experiments were performed to check the thermal stability of the sample, the influence of the TEM supporting grids and the effect of the electron beam on the reaction. The thermal stability of the $Zn_{0.92}Ga_{0.08}S$@CNTs was tested in high vacuum in the TEM at temperatures of up to 800 °C. Other than the presence of foreign particles decorating the external CNT surfaces (Figure S4a in the Supporting

[a] Dr. P. M. F. J. Costa
CICECO, Department of Ceramics and Glass Engineering
University of Aveiro, 3810-193 Aveiro (Portugal)
Fax: (+351) 234401470
E-mail: pedromfjcosta@ua.pt

[b] Dr. T. W. Hansen, Dr. J. B. Wagner, Prof. R. E. Dunin-Borkowski
Center for Electron Nanoscopy
Technical University of Denmark
2800 Kgs. Lyngby, (Denmark)

Supporting information for this article is available on the WWW under http://dx.doi.org/10.1002/chem.201001301.

Information), no structural or chemical alterations were observed. The contaminants were found to contain the transition metals Cr, Fe and Ni (Figure S4b in the Supporting Information) and were observed both in the blank runs and in the final oxidised products. Careful examination found these contaminants to originate from the holder furnace (Figure S5 in the Supporting Information). Their presence did not appear to influence the nanocable-to-nanotube transition. When comparing choices of TEM grids, it was found that bare, 300 mesh, Au grids were the most unreactive and free of contaminants under oxygen flow at high temperature. The effect of the 300 kV electron beam was also studied. In the absence of reactive gas, the structural stability of the nanocables was maintained if the electron density was lower than $6\times10^4\,e\,nm^{-2}s^{-1}$. Higher doses led to rapid deterioration of the carbon lattice, followed by decomposition of the core. In the presence of oxygen and at high temperature, the electron beam increased the reaction rate significantly and the dose had to be reduced ($<1\times10^3\,e\,nm^{-2}s^{-1}$). When combined with the holder instabilities that are characteristic of elevated temperature TEM studies, the implication of using such low doses was a limitation on imaging reactions at high spatial resolution (in spite of the presence of an aberration corrector). As a result, the reaction processes were mostly recorded at medium resolution. More detailed images were then acquired after stopping the reaction and evacuating the column (Figure S6 in the Supporting Information). To confirm that the electron beam did not have any further influence, several nanostructures were always kept unexposed until the final analysis of the product. These regions provided similar results to those obtained under controlled beam doses. Spectroscopic data were also collected using energy-dispersive X-ray (EDX) and electron energy-loss (EELS) measurements. Again, care was taken not to damage the material or to influence the oxidation reaction during these measurements.

The first set of experiments was carried out at the temperature used in the original report (550 °C). The nominal molecular oxygen flow was 4.8 mL min^{-1} resulting in a pressure of 5.8 mbar. Under these conditions, it was found that slow kinetics rendered the TEM study impractical. The temperature was therefore increased to 573 °C, which increased the reaction rate so that complete oxidation of a nanostructure could be achieved in less than 90 min. Figure 1a shows a $Zn_{0.92}Ga_{0.08}S$@CNT with an initial projected length of 1190 nm and a diameter of 130 nm. After 85 min of exposure (Figure 1b), the nanocable had been transformed entirely to a complex oxide nanotube with a diameter of 133 nm (an additional example of this nanocable to nanotube transition is given in Figure S7 in the Supporting Information). Continued exposure resulted in progressive growth of the nanograins (Figure 1c) in a manner similar to sintering. The rate of this process was further enhanced with additional increments in the temperature, leading to the formation of well-structured crystallites of ZnO along the tube (Figure 1d). The tubular interior was now difficult to distinguish, as the crystals grew both into and out of the wall. The

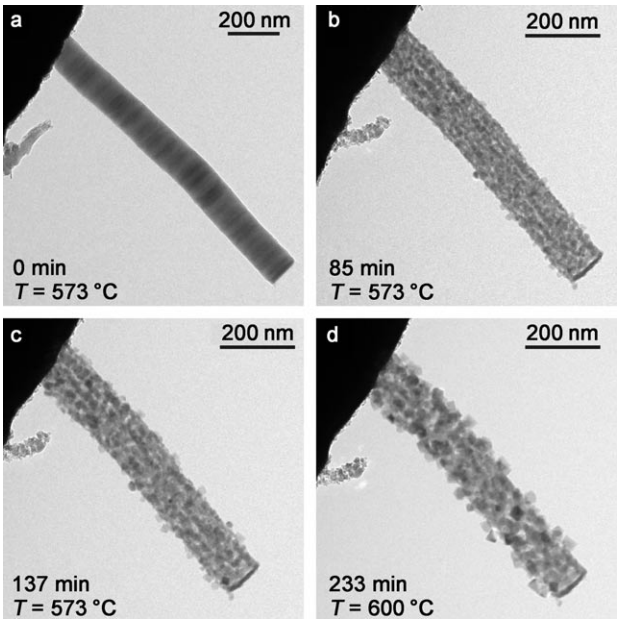

Figure 1. a)–d) Oxidation and sintering of a single $Zn_{0.92}Ga_{0.08}S$@CNT at a constant pressure of 5.8 mbar of O_2. Images b)–d) were taken at a specimen tilt angle of 23° (for optimal chemical analysis).

entire process of nanocable-to-nanowire transition followed by oxide nanograin sintering took more than 4 h (for this particular run).

Careful examination of the first stages of the reaction revealed that it proceeded through the formation of voids. These voids were generated close to the external surfaces, growing inwards until the sulfide core had been consumed (Figure 2a–d). This observation is consistent with the proposed mechanism based on the Kirkendall effect.

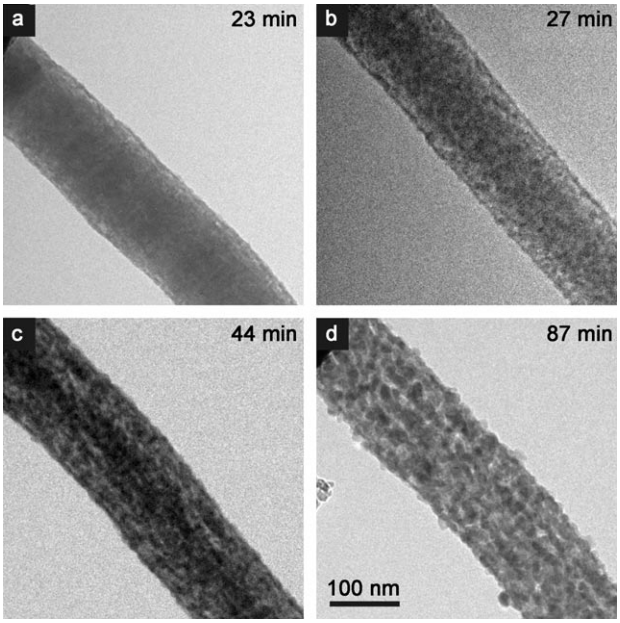

Figure 2. a)–d) Detail of the structure in Figure 1 showing the nanocable-to-nanotube transition. An oxide skin is visible in a) and b). All images were taken at the same magnification.

To gain further insight into the initial steps of the reaction, additional experiments were performed at a lower temperature (561 °C). The slower oxidation rate of the $Zn_{0.92}Ga_{0.08}S$@CNT then enabled the reaction to be stopped when the core started to oxidise. It also confirmed that the first step in the process is the depletion of the protective carbon shell (Figure 3a and b). When most of the carbon has been burnt and the sulfide starts to oxidise, surface-decorating platelets begin to form (Figure 3b), immediately before the formation of the voids (vacancy clusters) that are characteristic of the Kirkendall effect. Although the structures and compositions of these platelets are not well understood, high-resolution TEM images (Figure S6 in the Supporting Information) reveal an average lattice spacing of 0.29 nm, which is 15% smaller than that of the $\{10\bar{1}0\}$ planes in the doped ZnS core (0.34 nm). The platelets subsequently consolidate and the voids become visible (Figure 3c). Diffraction patterns confirm that growth of the oxide walls during the first stages of the reaction is epitaxial (Figure 3d and Figure S6 in the Supporting Information). In this case, the oxide lattice is contracted on average by 18% relative to that of the doped ZnS. As nanograins start emerging, the product increasingly becomes polycrystalline. Interestingly, the radius defined by the onset of the platelets marks the boundary for growth of the oxide tube. In this way, the oxide first grows on top of this oxide "skin". Eventually, the formation of a tubular wall composed of multiple oxide grains becomes noticeable as confirmed in Figure 3c and Figure S7 in the Supporting Information. Additional evidence for the formation of tubular structures was gathered by scanning electron microscopy (SEM) in the previous ex situ oxidation study.[8]

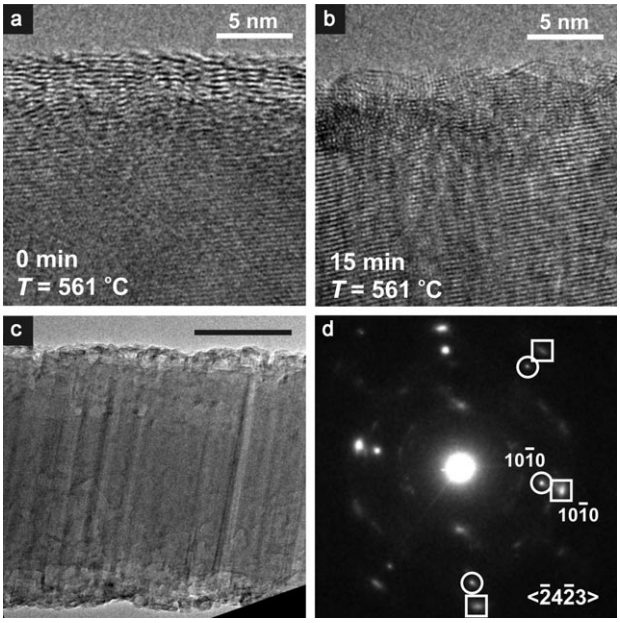

Figure 3. a) and b): High-resolution images detailing the first steps of the oxidation reaction. The carbon shell is removed selectively and replaced by an oxide "skin". c) Further into the reaction the effect of the coalescence of vacancies becomes visible. The scale bar is 50 nm. d) Diffraction pattern showing the coexistence of two lattices. Circles: sulfide; squares: oxide.

After full consumption of the core, sintering of the nanograins and subsequent growth of the zinc oxide crystallites takes place. It should be noted that the conditions employed here were not ideal for a comprehensive sintering behaviour study. In contrast to the analogous experiments carried out ex situ,[9] the operation of the ETEM under high-temperature reactive conditions required permanent vigilance. Additionally, harsher environments resulted in faster deposition rates of holder-derived contaminants. Generally, the in situ sintering process occurred uniformly along the length of the tubular structures giving rise to an assembly of nanoparticles with sizes in the same order of magnitude (Figure 1d). A deviation to this was the unique structure shown in Figure 4.

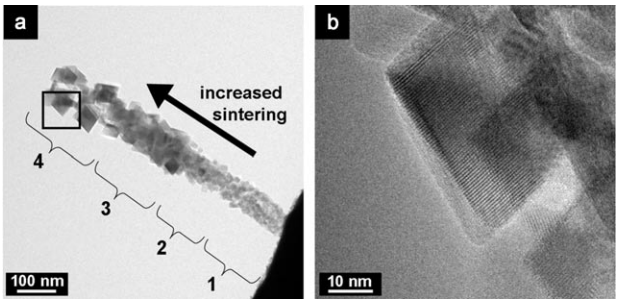

Figure 4. a) Oxidised nanotube after the sintering process. This unique structure illustrates the different sintering stages along its length. The four segments indicated on the image agree with the observed grain morphology evolution observed in ex situ sintering experiments. b) Magnified view of the crystallite boxed in segment 4.

Possibly due to localised variations of one or more experimental variables (temperature and gas pressure), the sintering of this nanotube generated a perfectly oriented arrangement of size-differentiated crystallites along its length. Although not representative (cf. Figure 1d), it suggests a path of prolonged sintering behaviour for the in situ experiments that is consistent with the observations gathered ex situ.[9] Notoriously, the gradual increase of the crystallites dimensions and random assembly of these along the nanotube's length is in strong contrast to the sintering behaviour of the core-shell $ZnO–TiO_2$ nanostructures observed by Yang et al.[10]

Within the collection of nanostructures studied in each run, the time required to change from a nanocable to a nanotube varied significantly. Considering the range of diameters of the initial materials this observation is not surprising, since larger nanocables would be expected to take longer to consume the core sulfide. The overall reaction rate was not dissimilar to that obtained using bench techniques, despite the lower gas flow and pressure used in the ETEM experiments.

As described in the original report,[8] opposite ends of the $Zn_{0.92}Ga_{0.08}S$@CNT nanocables differed in shape and structure. One end was typically straight and CNT-free with the sulfide core exposed, while the other end was usually hemispherical and enveloped by a carbon shell. This difference did not seem to influence the reaction. For structures in which both ends were visible, the depletion of the core appeared to proceed at similar rates at both ends.

It is now possible to conclusively describe the full oxidative process of $Zn_{0.92}Ga_{0.08}S$@CNT. First, the external carbon layers are consumed. When patches of sulfide become exposed, oxidation of the core is initiated. The formation of oxide platelets takes place at this stage, eventually forming an oxide "skin" that covers the sulfide core. This skin is expected to act as an insulating layer, preventing evaporation of the reactant species, as referred to in reference [3]. The Kirkendall effect then starts to dominate the process, with gradual removal of the core and a build-up of vacancies. Diffusion of the zinc cations, possibly along the pore wall surfaces, leads to net outward growth supported by the initial oxide skin. This step is followed by gradual growth of nanograins until the core is consumed.[7] Once a source of sulfur is no longer available, the grains start to diffuse and sinter until well-structured wurtzite-type ZnO crystallites are formed.

In conclusion, the Kirkendall effect has been imaged for individual nanostructures with high spatial and temporal resolution using $Zn_{0.92}Ga_{0.08}S$@CNT as an example of a model system. The experiments, which were performed in an environmental TEM, confirm that the mechanism proposed originally for the oxidation reaction appears to be correct. In particular, as a direct result of the enhanced visual and temporal control over the gas–solid reaction, it was possible to study the initial stages of the oxidation process. This capability helped to identify the elimination of the carbon shell and subsequent formation of an insulating oxide "skin" as the preceding steps to the Kirkendall effect.

Acknowledgements

U. K. Gautam, Y. Bando and D. Golberg are acknowledged for providing the sample. P.M.F.J.C. is grateful to the Royal Society of Chemistry for a JWT Jones Fellowship and CICECO for financial support. The A. P. Møller and Chastine Mc-Kinney Møller Foundation is gratefully acknowledged for their contribution towards the establishment of the Center for Electron Nanoscopy.

Keywords: carbon · chalcogenides · electron microscopy · Kirkendall effect · nanotubes

[1] A. D. Smigelskas, E. O. Kirkendall, *Trans. Am. Inst. Min. Metall. Pet. Eng.* **1947**, *171*, 130.
[2] Y. Yin, R. M. Rioux, C. K. Erdonmez, S. Hughes, G. A. Somorjai, A. P. Alivisatos, *Science* **2004**, *304*, 711.
[3] H. J. Fan, U. Gosele, M. Zacharias, *Small* **2007**, *3*, 1660.
[4] H. J. Fan, M. Knez, R. Scholz, K. Nielsch, E. Pippel, D. Hesse, M. Zacharias, U. Gosele, *Nat. Mater.* **2006**, *5*, 627.
[5] R. Ding, J. Liu, J. Jiang, Y. Li, Y. Hu, X. Ji, Q. Chi, F. Wu, X. Huang, *Chem. Commun.* **2009**, 4548.
[6] D. Tokozakura, R. Nakamura, H. Nakajima, J. G. Lee, H. Mori, *J. Mater. Res.* **2007**, *22*, 2930.
[7] R. Nakamura, G. Matsubayashi, H. Tsuchiya, S. Fujimoto, H. Nakajima, *Acta Mater.* **2009**, *57*, 5046.
[8] U. K. Gautam, Y. Bando, J. Zhan, P. M. F. J. Costa, X. S. Fang, D. Golberg, *Adv. Mater.* **2008**, *20*, 810.
[9] U. K. Gautam, Y. Bando, P. M. F. J. Costa, X. S. Fang, B. Dierre, T. Sekiguchi, D. Golberg, *Pure Appl. Chem.* **2010**, DOI: 10.1351/PAC-CON-09-12-08.
[10] Y. Yang, R. Scholz, H. J. Fan, D. Hesse, U. Goesele, M. Zacharias, *ACS Nano* **2009**, *3*, 555.

Received: May 13, 2010
Published online: September 6, 2010

